
Article:
Stephen, A.N. orcid.org/0009-0005-4471-080X, Holden, M.A. orcid.org/0000-0003-3060-7615, Sullivan, M.V. orcid.org/0000-0002-1771-8268 et al. (3 more authors) (2025) Optimised solution-phase synthesis of NanoMIPs for protein detection in electrochemical diagnostics. Biomedical Materials, 20 (2). 025043. ISSN 1748-6041

https://doi.org/10.1088/1748-605x/adb672

Optimised solution-phase synthesis of nanoMIPs for protein detection in electrochemical diagnostics

IOP Publishing Biomed. Mater. 20 (2025) 025043 https://doi.org/10.1088/1748-605X/adb672

Biomedical Materials

OPEN ACCESS

RECEIVED
28 October 2024

REVISED
4 February 2025

ACCEPTED FOR PUBLICATION
14 February 2025

PUBLISHED
10 March 2025

PAPER

Optimised solution-phase synthesis of nanoMIPs for protein detection in electrochemical diagnostics

AN Stephen[1], MA Holden[1], MV Sullivan[2,3], NW Turner[2], SR Dennison[1] and SM Reddy[1,*]

[1] Department of Chemistry, Institute of Materials and Investigative Sciences, UCLan Centre for Smart Materials, School of Pharmacy and Biomedical Sciences, University of Central Lancashire, Preston PR1 2HE, United Kingdom
[2] Department of Chemistry, University of Sheffield, Dainton Building, 13 Brook Hill, Sheffield S3 7HF, United Kingdom
[3] Micro/Bio/Nanofluidics Unit, Okinawa Institute of Science and Technology Graduate University, 1919-1 Tancha, Onna-son, Okinawa 904-0495, Japan
* Author to whom any correspondence should be addressed.

E-mail: smreddy@uclan.ac.uk

Keywords: molecularly imprinted polymers, nanoMIPs, affinity reagents, protein diagnostics, electrochemical

Supplementary material for this article is available online

Abstract

NanoMIPs are nanoscale molecularly imprinted polymers (MIPs) ranging in size between 30 to 300 nm offering a high affinity binding reagent as an alternative to antibodies. They are being extensively researched for applications in biological extraction, disease diagnostics and biosensors. Various methodologies for nanoMIP production have been reported demonstrating variable timescales required, sustainability, ease of synthesis and final yields. We report herein a fast (<2 h) method for one pot aqueous phase synthesis of nanoMIPs using an acrylamide-based monomer and N,N'-methylenebisacrylamide crosslinker. NanoMIPs were produced for a model protein template namely haemoglobin from bovine species. We demonstrate that nanoMIPs can be produced within 15 min. We investigated reaction quenching times between 5 and 20 min. Dynamic light scattering results demonstrate a distribution of particle sizes (30–900 nm) depending on reaction termination time, with hydrodynamic particle diameter increasing with increasing reaction time. We attribute this to not only particle growth due to polymer chain growth but based on AFM analysis, also a tendency (after reaction termination) for particles to agglomerate at longer reaction times. Batches of nanoMIPs ranging 400–800 nm, 200–400 nm and 100–200 nm were isolated using membrane filtration. The batches were captured serially on decreasing pore size microporous polycarbonate membranes (800–100 nm) and then released with sonication to isolate nanoMIP batches in the aforementioned ranges. Rebinding affinities of each batch were determined using electrochemical impedance spectroscopy, by first trapping nanoMIP particles within an electropolymerized thin layer. Binding constants determined for NanoMIPs using the E-MIP sensor approach are in good agreement with surface plasmon resonance results. We offer a rapid (<2 h) and scalable method for the mass production (40–80 mg per batch) of high affinity nanoMIPs.

1. Introduction

The immunodiagnostic sector constitutes a multi-billion-dollar industry [1], heavily reliant on the widespread availability and utilization of animal-derived monoclonal and/or polyclonal antibodies. Within this sector, there exists a significant demand for reliable synthetic receptor technologies capable of mimicking antibody binding affinities, particularly in detecting protein and viral biomarkers especially when antibodies are unreliable or are difficult to produce. Technologies, with the potential to replace traditional antibodies in disease diagnostics, bio-extraction and purification, include molecularly imprinted polymers (MIPs), which represent a rapidly evolving class of synthetic antigen-recognition materials. MIPs feature cavities or binding sites capable of selectively re-binding specific biomolecules

like protein antigens or viruses, offering an alternative to antibodies that are synthetically produced, stable, ethically sound, and cost-effective.

Acrylamide-based polymer hydrogels, extensively researched for their protein-selective properties, serve as a prominent example of MIPs. These hydrogels, produced using inexpensive reagents, can be synthesized in a single day through a one-pot process, resulting in micron-sized particles [2–5], thin films [6–9], and nanoscale particles [10–12] ranging from 50 to 200 nm. Our recent advances include the development of virus-imprinted MIPs for selectively capturing and neutralizing animal viruses [13]. Additionally, a MIP-based electrochemical sensor strategy has been demonstrated for the antibody-free determination of SARS-CoV-2 in saliva [14], with electrochemically produced MIPs showing promise for the detection of proteins at sub-nanomolar levels [15].

MIPs have been synthesised through various methods, involving either chemical or electrochemical initiation [15–17], resulting in suspensions of micro and/or nanoparticles in gel form within solutions [11, 18, 19] or as thin films [8, 20, 21]. IR spectroscopy of polyacrylamide-based MIPs have been previously reported showing the presence of amide functional groups [8]. It was also demonstrated in the same publication that hydrogen bonding interactions can occur between target protein and potential MIP binding sites. Traditionally, MIP synthesis has involved creating a monolith (bulk) MIP using acryloyl-based monomers like acrylamide [18], acrylic acid, and N-hydroxymethylacrylamide (NHMA) [8], leading to the formation of polymeric hydrogels. The polymer gel monolith is then mechanically broken down via manual sieving or grinding to generate micron-sized particles, exposing target-specific cavities on each particle's surface. However, due to the rudimentary nature of the grinding process, there is limited control over the physical characteristics of the final particles, resulting in the creation of random nanoscale features alongside the desired cavities. Consequently, MIPs produced in this manner exhibit minimal homogeneity and are susceptible to nonspecific binding, leading to lower binding affinities for the target.

Recent approaches have focused on the formation of nanoscale MIPs (nanoMIPs) on a solid phase employing a bottom–up methodology to create MIP particles that closely resemble the target in dimension [11, 19, 22–25]. This results in MIPs with higher affinity, as the binding sites exhibit a 'one-to-one' correspondence with the target protein. Two synthesis methods have been extensively explored; solid phase support synthesis and solution phase. With solid phase support, micrometre sized glass beads have been the favoured substrate [11]. The template molecule is chemically immobilised to glass beads which are then packed in a column. A reaction mixture consisting of functional monomers, crosslinker and initiators are then flowed through the column with subsequent nanoMIP growth occurring at the template-functionalised glass beads. After reaction quenching [11], the nanoMIPs selectively bound to the glass beads are released into solution and harvested using extended dialysis and lyophilisation. This a multi-step process taking at least 3 d to produce 18 mg of material. Albeit low yields, the method produces monodisperse particles with high affinity for target template. The solution phase microgel (MIG) method involves precipitation polymerisation where a very dilute polymer solution, the template and the crosslinker in solution is used. This polymerisation technique starts like the bulk monolith method however, it is stopped just before a bulk monolith hydrogel is formed by diluting the solution either with water or phosphate buffer saline (PBS) forming spherical nanoMIPs [26]. Others [27] have also developed a method that works in a similar way oil/water Pickering emulsions, using temperature responsive N-isopropylacrylamide (NIPAM) monomer and programmed ramped temperature changes and careful timing with the addition of the initiators to form these molecularly imprinted MIGs or nanoMIPs with an imprinting factor (MIP versus NIP) of 2:1. Herein we demonstrate that nanoMIPs can be produced at room temperature in aqueous solution. There can be a tendency to produce polydisperse particles sizes with varying affinities for target template. We address this here by using a series of nano-filters to size separate the nanoMIPs. We demonstrate a nanoMIP size dependency leading to higher affinities.

Despite offering superior affinities compared to the bulk MIP approach [18], both bulk MIP and nanoMIP methods face challenges in seamless integration with sensors. The layering of nanoMIPs onto sensor surfaces poses a significant challenge, necessitating additional surface chemical modifications. For instance, this can involve the use of 11-mercaptoundecanoic acid followed by a coupling procedure employing 1-ethyl-3-(3-dimethylaminopropyl) carbodiimide (EDC)/N-hydroxysuccinimide (NHS) to attach the MIPs to the sensor chip surface. The EDC/NHS methodology has been reported in sensor systems such as quartz crystal microbalance, surface plasmon resonance (SPR) chips, electrochemical electrodes, and screen-printed electrodes (SPEs) [28, 29]. We have addressed this here by physically entrapping the nanoMIP on an electrode in an electropolymerized thin-film matrix. Whereas both methods are appropriate for the attachment of nanoMIP to a gold electrode surface, there are several advantages for the physical trapping method we used. First, it is an electrochemical method allowing fine control of layer-by-layer deposition of an electrochemically grown layer (E-layer) in order to

physically entrap the nanoMIP particles [15]. Given the chemical nature of the E-layer used being like the nanoMIP, there is natural compatibility between the two materials ensuring facile integration and minimising rejection. With EDC/NHS chemical coupling, subsequent surface blocking steps are required to passivate the unused surface requiring ethanolamine and/or serum albumin as a blocking agent to minimise non-specific binding [30, 31]. However, with physical entrapping the E-layer formed around the nanoMIP particles offers a dual purpose of locking the nanoMIP down to the surface region and also passivating unused surface.

Efforts to scale up the production of functional nanoMIPs for commercial applications, such as diagnostics, imaging and biological extractions are ongoing. While some progress has been made, particularly with nanoMIPs using a MIG synthesis processes in solution, existing methods suffer from low milligram yields and lengthy (days) production times [27].

To address this, we have developed and improved these existing approaches to deliver a method with improved yields of high affinity protein-selective nanoMIPs that can be easily integrated with electrochemical sensors resulting in sub-picomolar determinations of target. Antibody-like affinity is confirmed by electrochemical determination of K_D. A comparison is made with K_D values determined using SPR.

Our advances represent a significant step toward addressing the scalability challenges associated with nanoMIP production, paving the way for broader adoption and application in various industries.

2. Experimental

2.1. Materials

N-hydroxymethylacrylamide (NHMA, 48% w/v), N,N′-methylenebisacrylamide (MBAm), phosphate buffered saline tablets (PBS, 10 mM, pH 7.4 ± 0.2), methylhydroquinone (MHQ), potassium ferricyanide ($K_3Fe(CN)_6$), potassium chloride (KCl), sodium nitrate ($NaNO_3$), potassium peroxydisulfate (KPS), sodium dodecyl sulphate (SDS), acetic acid (AcOH), ammonium persulphate, Tetramethylethylenediamine (TEMED), haemoglobin and serum albumin from bovine species, and buffers (PBS, HEPES and Tris) were all purchased from Merck Ltd Buffers were prepared in E-pure water (resistivity 18.2 ± 0.2 MΩ·cm). DropSens disposable SPEs (Au-AT & Au-BT) comprising a gold working electrode (4 mm diameter), a platinum counter electrode and silver reference electrode were purchased from Metrohm (Runcorn, Cheshire).

2.2. Nanogel (nanoMIP and nanoNIP) synthesis

Nanogels were synthesized via radical polymerization using N-hydroxyethylmethacrylamide (NHMA) as the monomer, bovine hemoglobin (BHb) or bovine serum albumin (BSA) as the template protein, and N,N'-methylenebisacrylamide (MBAm) as the cross-linker. Specifically, 1.080 g of NHMA, 0.24 g of BHb (or BSA), and 0.12 g of MBAm were dissolved in 20 ml of phosphate-buffered saline (PBS, pH 7.4) containing 0.0037 g sodium dodecyl sulphate (SDS). The solution was stirred continuously under a nitrogen atmosphere. Radical initiation was initiated by adding 400 µl of 10% (v/v) tetramethylethylenediamine (TEMED) and 5% (w/v) ammonium persulfate (APS). The reaction vessel was sealed with parafilm, leaving a 1 cm headspace to prevent pressure buildup, and the mixture was stirred vigorously for 1 min. The stirring rate was then reduced to 250 rpm, and aliquots (500 µl) of the reaction mixture were withdrawn at defined time intervals (5, 7, 10, 15, and 20 min). Each aliquot was immediately quenched with an equal volume (500 µl) of 10 mM methoxyhydroquinone (MHQ). Polymerization was monitored until the reaction mixture turned cloudy, indicating completion (approximately 20 min).

The polymerization products were analysed using a BioDrop μLITE UV–visible spectrometer to confirm polymer formation. Upon reaction completion, the remaining mixture was quenched with an excess of 20 ml of 10 mM MHQ.

2.3. Spectrophotometric characterisation of nanoMIP

NanoMIP synthesis was optimized for a 15 min reaction time. Aliquots (1 ml) of the reaction mixture were quenched, centrifuged at 15 000 rpm, and the supernatant discarded. The pelleted NanoMIPs were treated with 5 ml of a denaturing solution comprising 10% (w/v) SDS and 10% (v/v) acetic acid to elute the template protein. Following centrifugation (15 000 rpm), the supernatant was collected for spectrophotometric analysis at 395 nm, a wavelength chosen to account for the denatured protein's absorbance shift [18]. The washing/elution procedure was repeated five times, and subsequent washes with ultrapure water (⩾5 cycles) were conducted to remove residual SDS. The efficacy of SDS removal was confirmed by KCl precipitation tests [32]. Finally, the purified NanoMIPs were resuspended in 1 ml PBS.

An alternative protein elution method using sonication was also investigated. NanoMIPs were washed with ultrapure water and subjected to sonication at 30 °C for 15 min, followed by centrifugation and supernatant removal. This procedure was repeated five times, and the amount of eluted protein was analysed spectrophotometrically at 406 nm, a wavelength indicative of intact, non-denatured protein.

Following protein elution, NanoMIPs (1 ml) were reloaded with BHb (1 mg ml^{-1}) for 30 min to assess template protein rebinding. The percentage of protein rebound (%Rebind) was calculated spectrophotometrically (at 406 nm for BHb) using

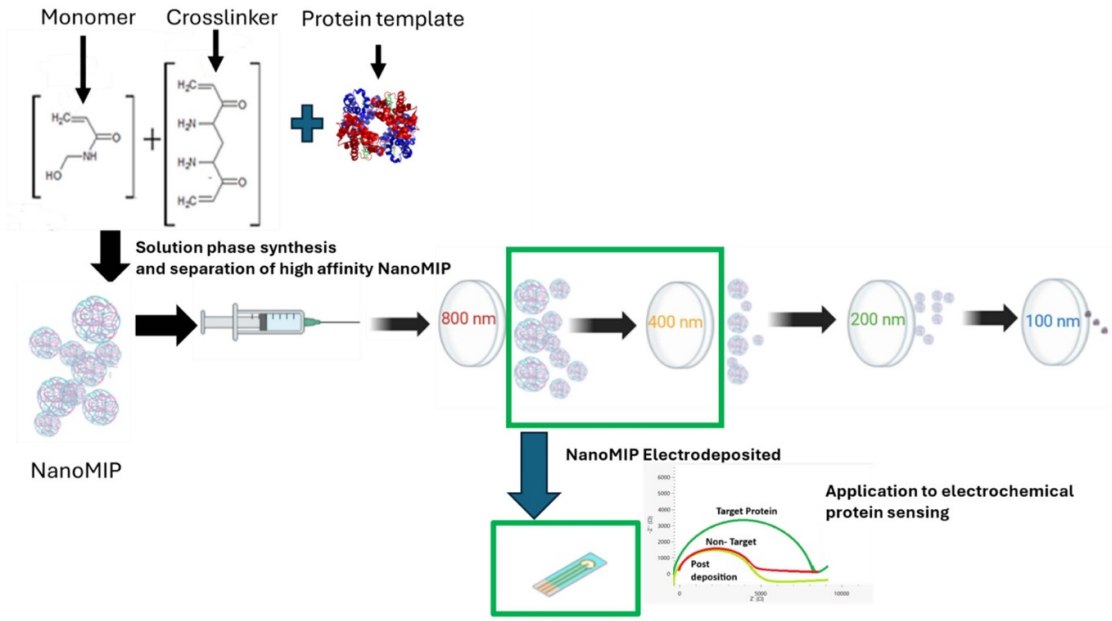

Figure 1. Schematic representation showing nanoMIP synthesis and subsequent isolation of different size nanoMIPs where the initial polydisperse mixture is passed though progressively smaller filters from 800–100 nm allowing for size selection of the produced nanoMIPs. Subsequent biosensor application of optimised nanoMIP illustrated.

the formula: %Rebind = 100 × (O–R/O), where O represents the initial protein concentration, and R represents the residual protein concentration post-rebinding.

2.4. Size selection of nanoMIPs using extrusion filtration

1 ml of the protein-eluted and sonicated nanoMIP mixture was taken through a mini extruder (Avanti Polar Lipids, Inc.) with decreasing filter sizes of 800–100 nm (2–5 min process for each filter size). Starting with the largest pore size filter (800 nm), the residue collected on the membrane was suspended into E-pure water (1 ml) using sonication. The filtrate was then sequentially passed through smaller filters repeating the same process, using 400, 200 and then 100 nm pore size membranes. The residue on the membrane thus collected at each stage were expected to give batches of particles ranging in size >800 nm (on 800 nm filter); 400–800 nm (on 400 nm filter); 200–400 nm (on 200 nm filter); 100–200 nm (on 100 nm filter); and <100 nm (the final filtrate). Each batch was lyophilised for subsequent dynamic light scattering size measurement and electrochemical characterisation. Figure 1 gives a summary of the process followed to obtain nanoMIPs at various filter sizes.

2.5. NanoMIP lyophilisation and yield determination

The nanoMIP solution flash frozen in liquid nitrogen followed by lyophilisation using a CHRIST Alpha 2–4 LDplus freeze-dryer. The Eppendorf tube, with opening covered with Parafilm® and pierced was then placed in the freeze dryer at −90 °C and at low pressure (0.011 mbar) until a fine fluffy off-white powder was produced (16 h). The mass of the lyophilised powder was then determined.

2.6. Dynamic light scattering characterization of nanoMIPs

The hydrodynamic size of NanoMIPs was determined using a Zetasizer Nano ZS. Lyophilized NanoMIPs were resuspended in PBS, and measurements were performed in triplicate using a disposable cuvette (refractive index: 1.32). The samples were equilibrated for 60 s prior to measurement.

2.7. Electrochemical deposition and analysis of nanoMIP

Electrochemical experiments were conducted using a Metrohm Autolab PGSTAT204 potentiostat with NOVA2.1.4 software. NanoMIP-modified electropolymerized layers (E-layers) were fabricated on BT-Au SPEs by cyclic voltammetry (CV), following a previously reported procedure [15]. A solution (50 µl) containing 0.1 mg NanoMIP, 641 mM NHMA, 41.5 mM MBAm, 0.29 M $NaNO_3$, and 48.15 mM KPS in PBS was deposited on the SPE surface (figure 1). Potential was cycled between −0.2 V and −1.4 V for 7 cycles at 50 mV s^{-1} (10 min, RT, 22 ± 2 °C). Control E-layers (without NanoMIPs) were also prepared.

The NanoMIP-modified electrodes were exposed to varying concentrations of BHb (100 fM–100 µM) for 5 min, followed by rinsing and analysis using electrochemical impedance spectroscopy (EIS) to assess

protein binding (figure 1). Selectivity was investigated using EIS in 5 mM potassium ferricyanide solution containing 0.5 M KCl, with data analysed using a Randles equivalent circuit model.

2.8. AFM images

AFM imaging of bare and NanoMIP-coated electrode surfaces was performed in liquid (PBS) using a Bruker Dimension Icon® with NanoScope 6 controller. PeakForce Tapping™ mode was employed with silicon nitride cantilevers (SCANASYST-FLUID, nominal spring constant 0.7 N m^{-1}). The coated electrodes were prepared as described in section 2.7 and imaged with and without NanoMIP entrapment.

2.9. SPR binding affinity studies

Using a Reichert 2 SPR system (Reichert Technologies, Buffalo, USA) SPR, experiments were performed using an adapted methodology, to provide accurate binding affinities of the imprinted materials. A carboxymethyl dextran hydrogel coated Au chips were installed as per the manufacturer's instructions. A running PBST (PBS pH 7.4 and 0.01% Tween 20) was flowed over the sensor surface at 10 µl min^{-1} until the baseline was stable, with this flow rate of 10 µl being maintained throughout the immobilisation process. For the immobilisation of the nanoMIP, a fresh solution of EDC (40 mg) and NHS (10 mg) dissolved in 1 ml water was injected onto the sensor chip surface for 6 min, this enables the activation of carboxyl groups contained within the carboxymethyl dextran layer. Next the nanoMIP (300 µg) dissolved in 1 ml of the running buffer (PBST) and 10 mM sodium acetate (0.82 mg ml^{-1}), was injected only to the left channel of the activated surface for 1 min. To deactivate the surface a quenching solution (1 M ethanolamine, pH 8.5) was then injected for 8 min enabling the deactivation of the carboxyl groups. This provide a sensor surface with nanoMIP immobilised onto the left channel as the working channel, while the right channel is used as a reference control.

Binding kinetic analysis performed using an existing methodology and initiated by injection of the running buffer PBST (blank) onto the nanoMIP immobilised sensor surface with a 2 min association, followed by a 5 min dissociation. The binding kinetics of the individual nanoMIPs towards the analyte (BHb) was determined from the association of analyte between 4–64 nM of BHb. After dissociation a regeneration buffer (10 mM Glycine-HCl, pH 2) was used to remove the analyte from the nanoMIP, thus renewing the sensor surface.

Signals from the working channel (left) were subtracted with those of the respective reference channel (right), to reveal the specific binding of the nanoMIP. The SPR responses were fitted using a 1:1 Langmuir bio-interaction (BI) model using TraceDrawer Software. Association rate constant (k_a), dissociation rate constant (k_d), and maximum binding (B_{max}) were fitted globally, whereas the BI signal was fitted locally. The equilibrium dissociation constant (K_D) was calculated from k_d/k_a.

3. Results and discussions

3.1. NanoMIP production and optimisation

Previously published MIG synthesis methods [33, 34] were adopted and modified for the preparation of nanoMIPs. We report for the first time the use of extrusion methods to size-select and purify nanoMIPs. Parameters such as synthesis time and use of a quenching agent were found to be important in delivering nanoparticles with reduced variability in average size according to DLS measurements. Aliquots were taken and reaction terminated using methylhydroquinone at each time point displayed. Figure 2 shows the averaged size for particles at each time point. Detectable particles were only produced after an initial lag of 5 min. It should be noted that even though the averaged hydrodynamic particle diameter was increasing with increased reaction time, it was clear from DLS measurements that a range of particle sizes were being produced throughout the process. Figures S1–S5 compare DLS spectra at time points 5, 7, 10, 15 and 20 min.

We attribute the presence of large particles at short reaction times to second order processes subsequent to chemical reaction where particles are tending to aggregate. The extent of aggregation increases with nanoMIP particle synthesis time. In order to minimise the concentration of large agglomerates, we selected the reaction termination time of 15 min.

Prior to any separation of particles into size batches, we looked to optimise protein elution and rebinding conditions of the parent batch. We demonstrate here a move away from using conventional harsh elution conditions with SDS/AcOH [18] to the application of sonication to release template protein from the nanoMIP. Sonication at 30 °C demonstrated an almost identical protein elution profile to using SDS/AcOH (figure 3(a)). Subsequent target rebinding studies demonstrated that sonicated nanoMIP was only 10% less effective at rebinding BHb than SDS/AcOH washed nanoMIP (figure 3(b)). Given the reduced need for reagents without significantly affecting rebinding properties, we selected the use of sonication and mild heating to elute the non-covalently bound target protein.

To further optimise rebinding conditions, we investigated the effect of buffer solution used on protein rebinding to nanoMIP. We investigated PBS, HEPES buffer and Tris buffer all at pH 7.4. Deionised water only was also tested. Figure 4 shows HEPES buffer was not an effective support medium for rebinding

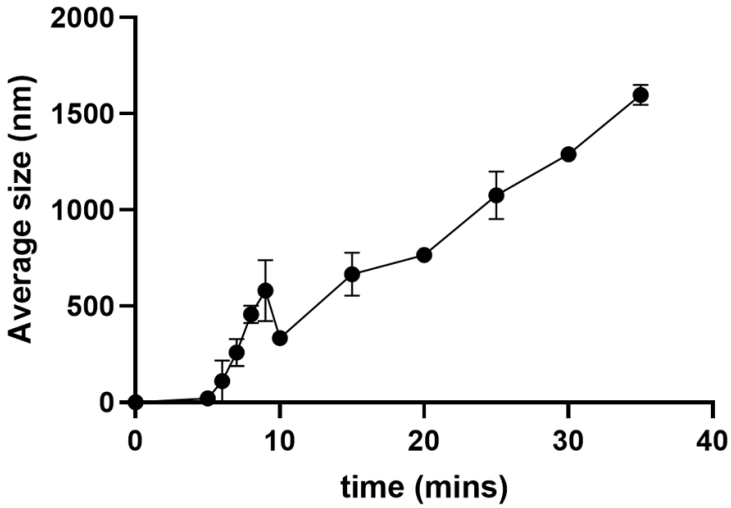

Figure 2. Increase in average gel hydrodynamic particle diameter with increasing synthesis time prior to MHQ quenching of reaction. Figures S1–S5 show a selection of representative DLS spectra at time points 5, 7, 10, 15 and 20 min synthesis times respectively. The synthesis was conducted in triplicate, yielding three DLS spectra per synthesis time. Each data point in figure is therefore the average hydrodynamic diameter from three sets of DLS spectra for each synthesis time (Data represents mean ± S.E.M., $n = 3$).

of protein to NHMA based nanoMIPs. PBS showed nanoMIPs to be 80% effective at protein rebinding whereas Tris buffer demonstrated that the nanoMIPs were 10% less effective than PBS and approximately 10% more effective that water only. The conformational stability of proteins has been known to increase if anionic buffers are used above the pI of the protein (and conversely, if cationic buffers are used below the pI) [35]. At its pI, a protein is electrically net neutral containing a balance in charge between carboxyl and amide groups existing as $–COO^-$ and $–NH_3^+$ respectively. Above their pI however, proteins become negatively charged and the groups exist as $–COO^-$ and $–NH_2$ respectively. BHb has a pI of 7.1 and therefore at pH 7.4 has an overall slight net negative charge. This overall negative net charge induces more favourable and complementary hydrogen bonding interactions between protein and the nanoMIP polymer At pH 7.4, the partially protonated phosphate buffer or the Tris buffer (pKa of 8.1) with its three un-dissociated hydroxyl groups appear suitable for improving MIP selectivity by providing optimum specific binding and reducing non-specific binding interactions. It is plausible that the PBS and Tris buffer systems are aiding in stabilising the native protein structure within the nanoMIP binding site. However, the poor rebinding of BHb with HEPES is remarkable. We propose that at the binding site of the nanoMIP, there is a net anionic repulsion between the protein and the prominent sulphonate group of HEPES buffer molecules resulting in poor capture of protein by nanoMIP. Due to optimum rebinding of protein in PBS, we used NHMA nanoMIPs in PBS going forward.

3.2. NanoMIP particle size selection and dynamic light scattering studies

We then investigated the effect of extrusion filtering (taking 2–5 min) through microporous polycarbonate membranes (800 to 100 nm) as a method to successively narrow the size range of nanoMIP particles in the parent sample (figure 1). The residue on the membrane thus collected at each stage were expected to give batches of particles ranging in size greater than 800 nm (on 800 nm filter); 400–800 nm (on 400 nm filter), 200–400 nm (on 200 nm filter) and 100–200 nm (on 100 nm filter). The final filter used was 100 nm in pore size ensuring the filtrate contained only particles of less than 100 nm. Each batch and the final filtrate were lyophilised for subsequent dynamic light scattering size measurement and electrochemical characterisation. A fraction (0.1 mg) of each lyophilised sample was resuspended in PBS for DLS analysis. Figure 5 shows the effect of using various pore sized polycarbonate filters to isolate nanoMIPs. The filtration technique was effective in minimising aggregation of particles.

Whilst the plot in figure 5 gives a snapshot average of the hydrodynamic particle diameter in any fraction collected, the real situation is best captured from the raw DLS data (figures 6(a)–(e) which show a range of hydrodynamic particle diameters for each collected residue (unfiltered material) and the final filtrate. Figure 6(a) analyses the unfiltered material following filtration of nanoMIP crude sample through a 800 nm filter. Figure 6(a) shows a multimodal distribution of nanoMIP hydrodynamic particle diameters collected by the 800 nm filter suggesting that the larger particles (>800 nm) were blocking the filter and impeding

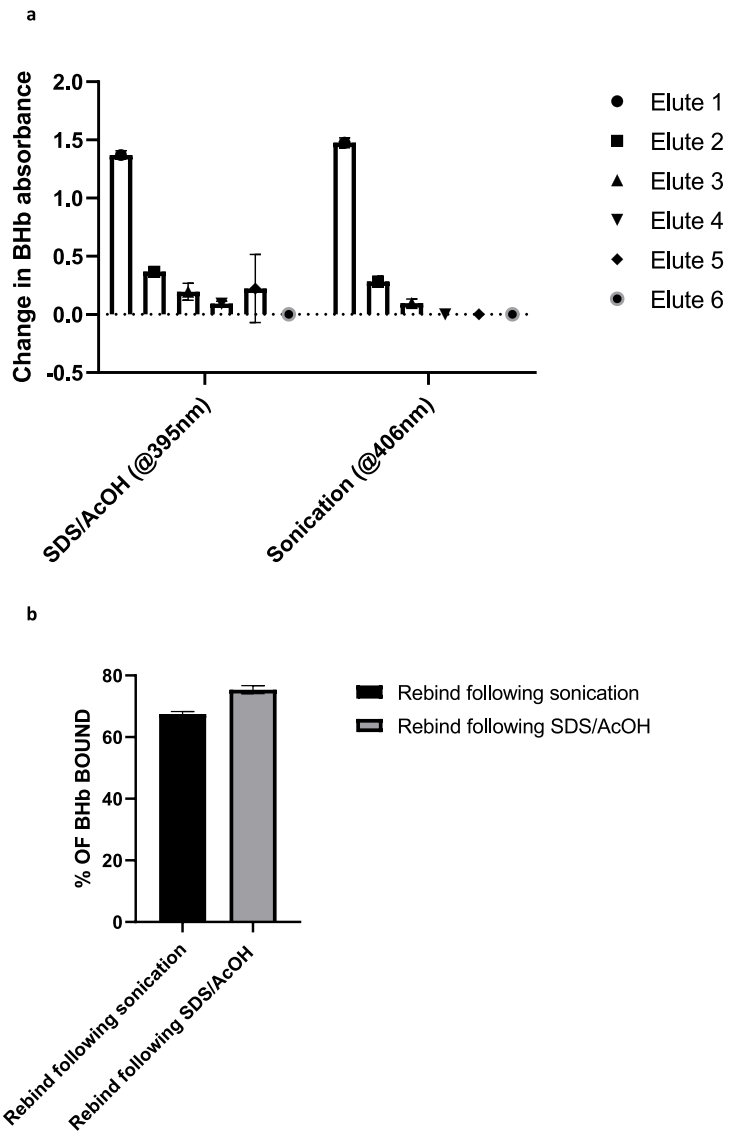

Figure 3. Comparison of the effect of SDS/AcOH and sonication with mild heating on (a) protein elution and (b) subsequent protein rebinding in PBS. % rebind was determined spectrophotometrically (at 406 nm for BHb) by measuring amount of protein remaining in solution after rebind (R) and comparing against original protein reload (O) using the equation $100 \times (O–R/O)$. Data represents mean ± S.E.M., $n = 3$.

the permeation of some (but not all) of the smaller particles. Figure 6(b) analyses the unfiltered material following filtration of the 800 nm filtrate through a 400 nm filter. We observe a bimodal distribution of nanoMIP particles in the range 30–100 nm and a very broad peak in the range 110–800 nm. Figure 6(c) analyses the unfiltered material following filtration of the 400 nm filtrate through a 200 nm filter. Again, we observe a similar bimodal distribution of nanoMIP particles sizes. Figure 6(d) analyses the unfiltered material following filtration of the 200 nm filtrate through a 100 nm filter. Here we observe a single peak between 100–200 nm centred around 150 nm indicative of a homogeneous nanoMIP particle size. And finally, figure 6(e) analyses the final filtrate emanating from the 100 nm filter. Interestingly, we observe a bimodal distribution of very small nanoMIP particles centred at 1.0 and 20 nm. However, the intensity of the peak at 1.0 nm is small representing an insignificant yield of particles and can be discarded.

3.3. Electrochemical binding affinity studies

The next stage was to test the rebinding affinity of each batch. Whereas the unfiltered parent batch was easy to pellet for UV/Vis characterisation of rebinding, the filtered batches (<800 nm) did not pellet. In order to test the rebinding efficiency of these particles, we used a modified form of our previously published electrochemical method [15]. In our previous method, we produced electrochemically grown thin film MIPs on disposable SPEs selective to target proteins. We used acrylamide-based monomers and the resulting thin film itself was the MIP. Rebinding of protein was evaluated using EIS in the presence of ferrocyanide as redox marker. The increase in charge transfer resistance

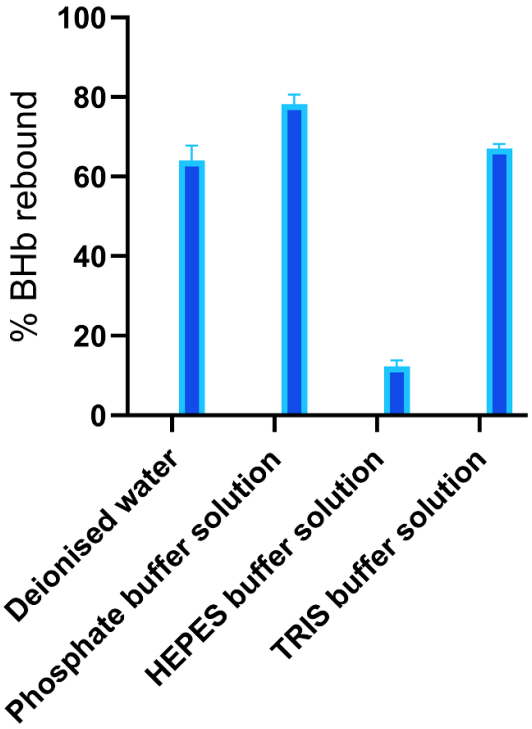

Figure 4. Effect of buffer composition on % target protein rebinding on BHb nanoMIPs. % rebind was determined spectrophotometrically (at 406 nm for BHb) by measuring amount of protein remaining in solution after rebind (R) and comparing against original protein reload (O) using the equation 100 × (O–R/O). Data represents mean ± S.E.M., $n = 3$.

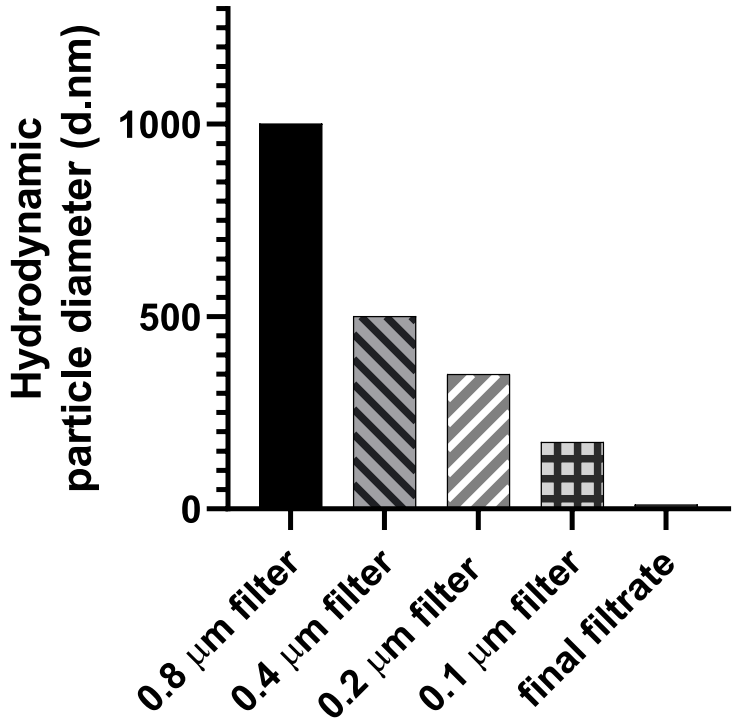

Figure 5. DLS particle sizing of fractions collected on sequential filters with decreasing pore size (800 to 100 nm) and final filtrate emanating from the last filter (100 nm). Fractions collected on each subsequent filter were sonicated and resuspended in buffer prior to DLS sizing. The filtrate from the filter was then passed through the next filter down and the collection/DLS process repeated.

(R_{CT}) was directly proportional to increased target protein binding. Here, we adapted this method by using the electrochemically produced thin film method to physically entrap nanoMIP at the electrode surface. One hundred microgrammes of each lyophilised batch was resuspended in 1000 µl of PBS

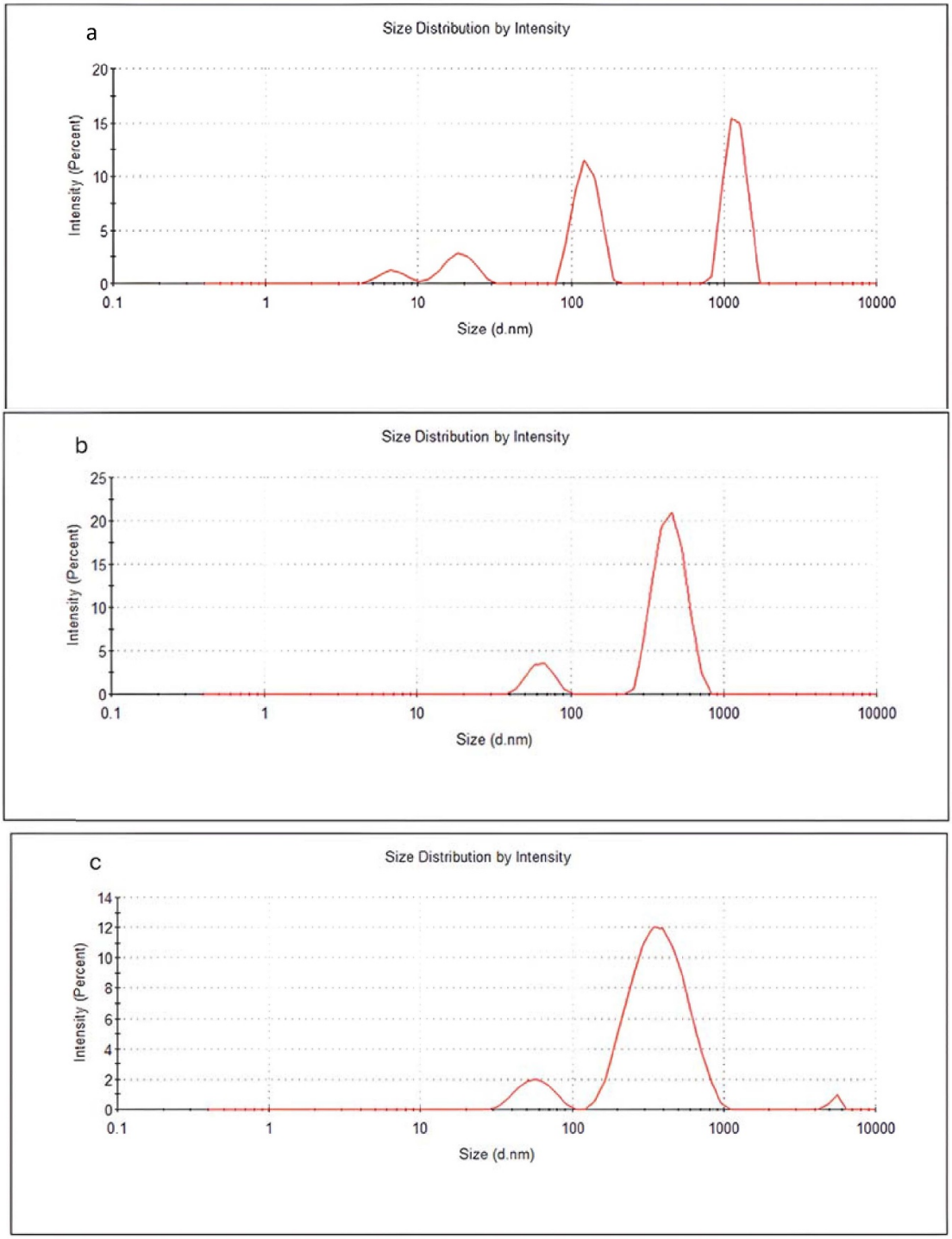

Figure 6. DLS spectra of fractions collected on sequential filters with decreasing pore sizes showing nanoMIP hydrodynamic particle diameter distribution for (a) 800 nm, (b) 400 nm (c) 200 nm and (d) 100 nm; and (e) final filtrate emanating from the last filter (100 nm).

containing NHMA monomer, bisacrylamide cross-linker and potassium persulphate (KPS) initiator. CV was used with a reduction cycle between −0.2 to −1.2 V to electrochemically induce KPS to produce sulphate radicals (SO_4^-) which in turn initiated chemical polymerisation of NHMA/bisacrylamide at the electrode surface. Seven cycles were used to produce a thin film that physically entrapped nanoMIPs *in-situ* (see figure S6). Figure 7(a) shows AFM of a bare gold electrode surface. Whereas the E-layered electrode is relatively smooth with few discernible features in the absence of nanoMIP (figure 7(b)), in the presence of nanoMIP captured on a 200 nm membrane (figure 7(c)), many particles are observable typically ranging in size from 100 to 200 nm, with some larger particles measured with heights greater than

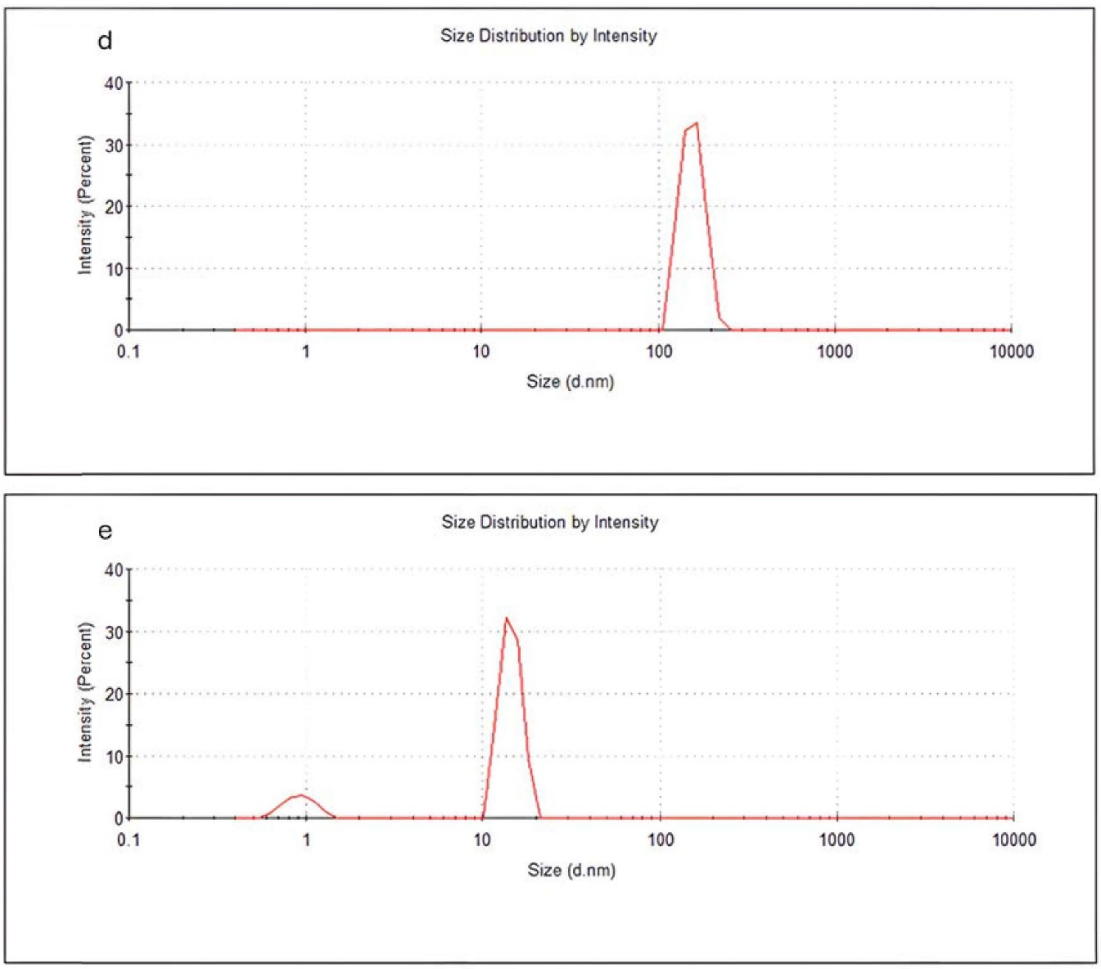

Figure 6. (Continued.)

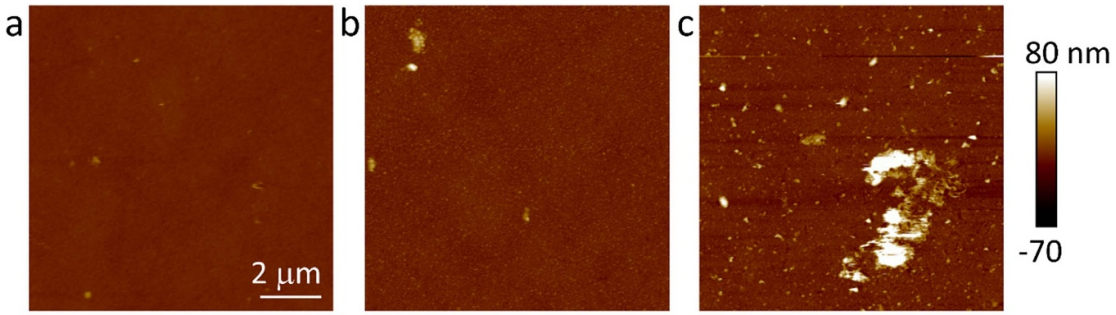

Figure 7. AFM micrographs of gold electrode (a), gold electrode E-layer surface in the absence of entrapped nanoMIP (b) and gold electrode E-layer surface in the presence of entrapped nanoMIP (c).

900 nm. We believe that the large particles are the result of some aggregation or coalescence of smaller nanoparticles (figure S7).

The nanoMIP entrapped E-layer was tested for target and non-target protein rebinding. We observed a concentration dependent change in R_{CT} from 1pM to 1 nM target protein addition (figure 8(a)). In the presence of non-target protein over the same concentration range there was a much-reduced signal (figure 8(b)). For example, at 1 nM protein level, the selectivity factor (response to target divided by response to non-target) was acceptable at 3:1.

The sensor LOQ was determined to be 1 pM, with an LOD of 100 fM. The signal plateaued beyond 10 nM and indicated that saturation in selective surface binding had occurred. Further, we investigated using the Hill-Langmuir method to determine K_D for nanoMIP. Assuming the latter was the maximum protein binding capacity of the E-MIP thin

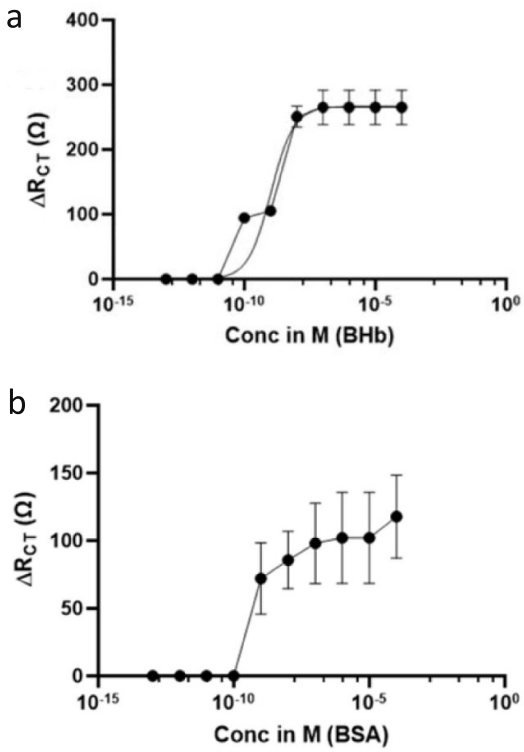

Figure 8. Concentration dependent change in R_{CT} for target, BHb (a) and non-target, BSA (b) binding to BHb NanoMIP. Data represents mean ± S.E.M., $n = 3$. Figure S8 shows the cumulative Nyquist plot data from which the R_{CT} was calculated. In each Nyquist plot there is a semi-circle arc, the diameter of which is indicative of the charge transfer resistance (R_{CT}) value. R_{CT} gives an indication of the ease with which the electrolyte and redox marker can be transported to the electrode surface.

film (B_{max}), we can use the Hill–Langmuir method to determine the equilibrium dissociation constant K_D for the E-MIP. We assumed the Hill coefficient is equal to 1, which is indicative of ligand (MIP) binding with no cooperativity to one site. The K_D was then determined from the plot to be the protein concentration associated with 50% of binding sites being occupied ($B_{max}/2$). The calculated K_D was determined to be 1.03 ± 0.4 nM.

Subsequently, each of the larger filtered batch sizes of nanoMIP were investigated electrochemically for yield, rebinding and selectivity using E-layer entrapment. Table 1 summarises the results. Some of the material collected on the 800 nm filter was prone to excessive clumping and sedimented immediately even after sonication. Whereas the yield was high (4.6 mg ml^{-1}) the material characterised for this fraction was very much representative of a mixed phase of particles ranging in size 100 to >800 nm giving low selectivity overall when tested on the electrochemical sensor. Selectivity was optimum when using the nanoMIP material collected on the 400 nm filter (representing material captured that has a biomodal distribution of hydrodynamic particle diameters centred at 110 and 800 nm; see figure 6(b)) and with acceptable yield (2 mg ml^{-1}). Filter fractions using 200 and 100 nm filters also gave acceptable selectivities. The worst performer in terms of selectivity was the 800 nm filter residue and the worst performer for yield was the final filtrate through the 100 nm filter. The latter is understandable given that particles at the lower filter size end are represented in the yields for the larger filter captures. We surmise that excessive filtration is not necessary and a two-stage filtration process using only the 800 nm followed by the 400 nm filters is required to deliver high selectivity materials.

3.4. SPR binding affinity studies

For a comparison to be made between the above electrochemical method for determination of K_D and the generally accepted SPR method, the binding of the prepared nanoMIPs were investigated for their affinity towards the target protein (BHb) using SPR in a running buffer of PBS (pH 7.4) and Tween 20 (0.01%). The lyophilised nanoMIPs collected from the 200 nm filter were resuspended in 1 ml of the running buffer, with the addition of sodium acetate, before being deposited onto the SPR chip (coated in a carboxymethyl dextran layer). Deposition of the nanoMIPs onto the SPR chip surface is achieved through standardised carbodiimide coupling via an adapted Steglich esterification [36, 37] and occurs due to the high percentage of hydroxyl-functionality contained within the polymer composition of the nanoMIP. The pre-functionalization of the gold SPR chips with a carboxymethyl dextran hydrogel layer enables for a good deposition profile, owing to the ease of activation of the dextran hydrogel by EDC/NHS. Ethanolamine is then used to deactivate any unwanted and unreacted carboxyl groups on the SPR chip surface, whilst also washing away any unbound nanoMIPs. Consistent with previous SPR-MIP binding studies, the initial deposition of nanoMIPs was added in excess to allow for full coverage on the chip, giving the maximum potential population of binding sites available per chip [38]. Thus, having a theoretical maximum receptor (binding population) allows for standard model for ligand/receptor interactions to be applied, enabling the application of a 1:1 kinetic binding model [39].

The SPR sensorgrams presented in figure 9 shows the interactions of five different concentrations of the target molecule (BHb) with two batches of the nanoMIPs collected from the 200 nm filter, labelled Batch 1 and Batch 2 (figures 9(A) and (B), respectively), immobilised onto the surface of the SPR chip. From these curves and the application of a 1:1 model the elucidation of the overall equilibrium dissociation constant (K_D) for the target interacting with their nanoMIPs and is summarised in table 2. SPR binding affinity studies could only be performed

Table 1. Effect of filter size on final yield and selectivity of nanoMIP. NanoMIP selectivity was determined by taking a ratio of electrochemical signal (ΔR_{CT}) for target (BHb) and non-target (BSA) protein binding.

Filter used to collect nanoMIP fraction	Yield (mg ml^{-1})	Selectivity at 100 nM (target = BHb; non-target = BSA)	Predominant NanoMIP size (nm)
800 nm	4.6	2:1	>800
400 nm	2	16:1	400–800
200 nm	2.6	8:1	200–400
100 nm	0.4	6:1	100–200
Final filtrate	0.2	6:1	1–100

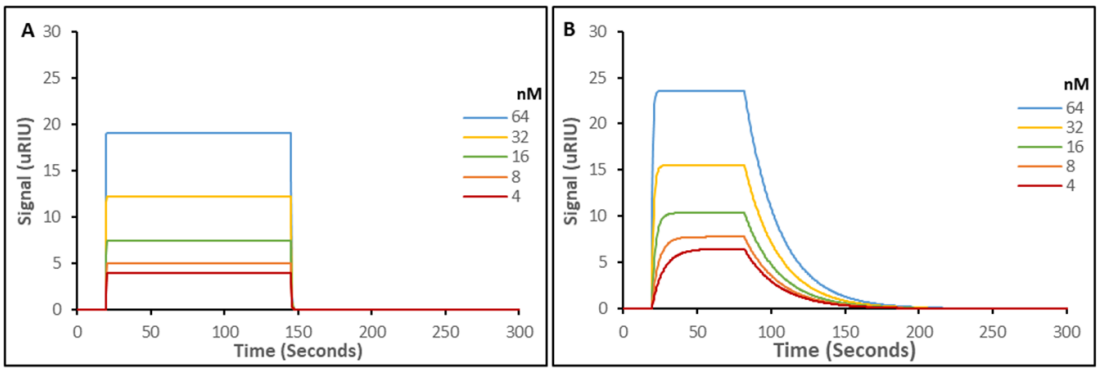

Figure 9. Representative SPR curves showing the rebinding of the target protein (BHb) to the immobilised nanoMIPs. Five concentrations of analyte in PBST. (A) BHb binding to BHb-imprinted nanoMIP (Batch 1); (B) BHb binding for BHb-imprinted nanoMIP (Batch 2).

Table 2. Calculated equilibrium dissociation constant (K_D) of the imprinted nanomaterials, from data presented in figure 9 and S9. All experiments were performed under ambient conditions. Data represents mean ± S.E.M., $n = 3$.

	K_D value (M)	
NanoMIP	BHb	BSA
Batch 1	2.75×10^{-9} ($\pm 0.85 \times 10^{-9}$)	6.21×10^{-7} ($\pm 0.23 \times 10^{-6}$)
Batch 2	2.20×10^{-9} ($\pm 0.20 \times 10^{-9}$)	2.64×10^{-7} ($\pm 0.02 \times 10^{-6}$)

on the 200 nm filtered batch simply because the SPR penetration depth will not be able to reach the surface of the 400 and 800 nm filtered batches of nanoMIPs. The penetration depth of traditional SPR chips is approximately 216 nm [40]. There have been significant advances in SPR chip production that have allowed the penetration depths to increase [41]. However, increasing sensitivity to allow for a greater probing depth has yet to reach the limit of greater than 400 nm. To explore specificity of the nanoMIP, the cross-reactivity and non-specific binding was also investigated through the loading of a non-target protein (BSA) onto the nanoMIP coated chip. The K_D values for the binding of the non-target (BSA), is also represented in table 2, with SPR sensorgrams shown in figure S9.

The interactions of the target protein (BHb) and the corresponding nanoMIPs were calculated with K_D values shown to be 2.75 and 2.20 nM, for the Batch 1 and Batch 2 nanoMIP, respectively. These values show consistency within synthesis of these, with batch-to-batch reproducibility. These K_D values are also consistent with our electrochemical method of determination (1.03 nM) requiring simple physical (E-layer) entrapment of nanoMIPs on an electrode which obviates the need for EDC/NHS coupling reagents. The values are also consistent with nanoMIPs, that have been produced using the more popular solid-phase synthesis methodology [11]. These studies show nanoMIPs produced via the solid-phase synthesis to consistently produce binding affinities (K_D values) in the nanomolar range, for protein targets such as trypsin and α-casein [39, 42, 43]. With SPR being used as the 'gold' standard to measure biomolecular interactions [44], the K_D values offered by the nanoMIPs produced in this study are shown to be consistent with that of monoclonal antibodies, which typically have K_D values within the low nanomolar to sub-nanomolar range [45], thus showing these synthetic recognition materials offer excellent recognition to a chosen target [10]. The nanomolar binding affinities (K_D values) produced by nanoMIPs is to be expected as highlighted by Silva *et al* due to their small size and large surface area and porosity, leading to more consistent and usability synthetic recognition material [46].

Evaluation of the nanoMIPs to discriminate between the target protein (BHb) and other proteins was investigated through the challenging of the non-imprinted protein (BSA), chosen due to the approximate size and hydrophobic solvent accessible surface areas and as a representative protein found in complimentary complex matrices. The SPR analysis shown in figure S9 reveals that there is some binding of the BSA to both batches of nanoMIP materials, but with vastly reduced affinity, with K_D values of 62.1 and 26.4 μM, for Batch 1 and Batch 2, respectively. This shows that both batches, as expected are selective for the template, with K_D values showing an approximate 100–200-fold improvement for the target protein (BHb) versus the non-target protein (BSA). This ratio of $K_{D\,BHb}/K_{D\,BSA}$ shows that these materials consistently bind more BHb compared with BSA.

Therefore, using our non-solid phase synthesis method with subsequent filtration, we are able to produce 2–5 mg yields of high affinity size selected nanoMIPs in less than 2 h. It should be noted though that this synthetic method to produce nanoMIPs requires high levels of target protein template (12 mg) to be used per synthesis, which is ultimately lost during the washing processes. Whereas this method would not be cost-prohibitive to produce MIPs for proteins of high abundance and low-cost, the method does not readily lend itself in the case of protein targets which are costly to produce. However, based on our investigation of a less harsh (sonication) method used to elute protein (rather than the generally accepted chemical denaturation method using SDS/AcOH [18]) we have the opportunity to recover non-denatured protein for re-use. This requires further investigation. In order to address the need to re-use protein template, other workers have used solid-phase synthesis methods, with target protein attached to glass beads [11] or silane coated magnetic beads [47] but these methods are often laborious and time-consuming. In an optimised solid phase method [19, 48] we recently reported an unprecedented nanoMIP yield of 50 mg ml^{-1} per day. To complement solid phase methods, we now offer a solution phase method to produce and harvest high (2–4 mg ml^{-1}) yields of high affinity nanoMIPs within 2 h; in a 20 ml reaction volume this equates to 40–80 mg of high affinity material per synthesis batch. An additional advantage is the single monomer required here compared with other nanoMIP methods which can use as many as 4 monomers in their procedures [11].

4. Conclusions

We demonstrate a rapid and simple solution phase synthesis method to produce nanoMIPs with hydrodynamic particle diameters ranging 30 to >800 nm and a total yield of 12 mg ml^{-1} in less than 1 h. Using a subsequent 2–5 min process, we are additionally able to size separate nanoMIPs into batches using a sequential range (800–100 nm) of polycarbonate membrane filters. NanoMIP rebinding capability and selectivity are a function of particle size. We surmise that excessive filtration is not necessary and a two-stage filtration process using only the 800 nm followed by 400 nm filters is required to harvest high selectivity materials (40–80 mg per 20 ml batch). The nanoMIPs are easily integrated to an electrochemical electrode sensor and we demonstrate nM sensitivity for target (BHb) protein with an acceptable selectivity of 16:1 when compared against a non-target protein. The electrochemical sensor method shows versatility for simple nanoMIP entrapment and sensor application. We also demonstrate for the first time that there is good correlation between the E-layer nanoMIP (electrochemical) method and SPR method to determine K_D.

Data availability statement

All data that support the findings of this study are included within the article (and any supplementary files).

Acknowledgment

SMR, ANS, SRD and MAH are grateful to the University of Central Lancashire, Royal Society of Chemistry COVID-19 Action fund (H20-188); RSC Research Enablement Grant (E22-5899202825), the Daiwa Anglo-Japanese Foundation (13094/13916) and The Royal Society (IES\R3\193093) for funding this work. NT and MS would like to thank the University of Sheffield and Engineering and Physical Sciences Research Council (EPSRC) for financial support for this work (EP/V046594/2).

Author contribution

SMR (@UCLan) conceived and directed the research and wrote the manuscript. ANS (@UCLan) performed NanoMIP synthesis, characterisation, and electrochemical studies. SRD (@UCLan) supported with the extrusion method used. MAH (@UCLan) performed AFM studies. NT (@Sheffield) and MS (@OIST) performed SPR measurements. All read and reviewed the manuscript.

ORCID iDs

AN Stephen https://orcid.org/0009-0005-4471-080X
MA Holden https://orcid.org/0000-0003-3060-7615

MV Sullivan https://orcid.org/0000-0002-1771-8268
NW Turner https://orcid.org/0000-0002-9380-5291
SM Reddy https://orcid.org/0000-0002-7362-184X

References

[1] Ecker D M, Jones S D and Levine H L 2015 The therapeutic monoclonal antibody market *mAbs* **7** 9–14
[2] El-Sharif H F, Hawkins D M, Stevenson D and Reddy S M 2014 Determination of protein binding affinities within hydrogel-based molecularly imprinted polymers (HydroMIPs) *Phys. Chem. Chem. Phys.* **16** 15483–9
[3] Boonpangrak S, Whitcombe M J, Prachayasittikul V, Mosbach K and Ye L 2006 Preparation of molecularly imprinted polymers using nitroxide-mediated living radical polymerization *Biosens. Bioelectron.* **22** 349–54
[4] El-Sharif H F, Phan Q T and Reddy S M 2014 Enhanced selectivity of hydrogel-based molecularly imprinted polymers (HydroMIPs) following buffer conditioning *Anal. Chim. Acta* **809** 155–61
[5] Ye L, Yu Y and Mosbach K 2001 Towards the development of molecularly imprinted artificial receptors for the screening of estrogenic chemicals *Analyst* **126** 760–5
[6] Schmidt R H and Haupt K 2005 Molecularly imprinted polymer films with binding properties enhanced by the reaction-induced phase separation of a sacrificial polymeric porogen *Chem. Mater.* **17** 1007–16
[7] Schmidt R H, Mosbach K and Haupt K 2004 A simple method for spin-coating molecularly imprinted polymer films of controlled thickness and porosity *Adv. Mater.* **16** 719–22
[8] Sullivan M, Dennison S, Hayes J and Reddy S 2021 Evaluation of acrylamide-based molecularly imprinted polymer thin-sheets for specific protein capture—a myoglobin model *Biomed. Phys. Eng. Express* **7** 045025
[9] Sullivan M V, Nanalal S, Dean B E and Turner N W 2024 Molecularly imprinted polymer hydrogel sheets with metalloporphyrin-incorporated molecular recognition sites for protein capture *Talanta* **266** 125083
[10] Poma A, Guerreiro A, Whitcombe M J, Piletska E V, Turner A P F and Piletsky S A 2013 Solid-phase synthesis of molecularly imprinted polymer nanoparticles with a reusable template–"plastic antibodies" *Adv. Funct. Mater.* **23** 2821–7
[11] Canfarotta F, Poma A, Guerreiro A and Piletsky S 2016 Solid-phase synthesis of molecularly imprinted nanoparticles *Nat. Protocols* **11** 443–55
[12] Sullivan M V, Fletcher C, Armitage R, Blackburn C and Turner N W 2023 A rapid synthesis of molecularly imprinted polymer nanoparticles for the extraction of performance enhancing drugs (PIEDs) *Nanoscale Adv.* **5** 5352–60
[13] Graham S P, El-Sharif H F, Hussain S, Fruengel R, McLean R K, Hawes P C, Sullivan M V and Reddy S M 2019 Evaluation of molecularly imprinted polymers as synthetic virus neutralizing antibody mimics *Front. Bioeng. Biotechnol.* **7** 115
[14] El Sharif H F, Dennison S R, Tully M, Crossley S, Mwangi W, Bailey D, Graham S P and Reddy S M 2022 Evaluation of electropolymerized molecularly imprinted polymers (E-MIPs) on disposable electrodes for detection of SARS-CoV-2 in saliva *Anal. Chim. Acta* **1206** 339777
[15] Stephen A N, Dennison S R, Holden M A and Reddy S M 2023 Rapid sub-nanomolar protein determination in serum using electropolymerized molecularly imprinted polymers (E-MIPs) *Analyst* **148** 5476–85
[16] Leibl N, Duma L, Gonzato C and Haupt K 2020 Polydopamine-based molecularly imprinted thin films for electro-chemical sensing of nitro-explosives in aqueous solutions *Bioelectrochemistry* **135** 107541
[17] Phonklam K, Wannapob R, Sriwimol W, Thavarungkul P and Phairatana T 2020 A novel molecularly imprinted polymer PMB/MWCNTs sensor for highly-sensitive cardiac troponin T detection *Sens. Actuators* B **308** 127630
[18] Hawkins D M, Stevenson D and Reddy S M 2005 Investigation of protein imprinting in hydrogel-based molecularly imprinted polymers (HydroMIPs) *Anal. Chim. Acta* **542** 61–5
[19] Reddy S M, Stephen A N, Holden M A, Stockburn W J and Dennison S 2024 Magnetic nanoparticle facilitated rapid mass production of high affinity polymeric materials (nanoMIPs) for protein recognition and biosensing *Biomater. Sci.* **12** 5845–55
[20] Tai D-F, Jhang M-H, Chen G-Y, Wang S-C, Lu K-H, Lee Y-D and Liu H-T 2010 Epitope-cavities generated by molecularly imprinted films measure the coincident response to anthrax protective antigen and its segments *Anal. Chem.* **82** 2290–3
[21] Kan X, Xing Z, Zhu A, Zhao Z, Xu G, Li C and Zhou H 2012 Molecularly imprinted polymers based electrochemical sensor for bovine hemoglobin recognition *Sens. Actuators* B **168** 395–401
[22] Hix-Janssens T, Davies J R, Turner N W, Sellergren B and Sullivan M V 2024 Molecularly imprinted nanogels as synthetic recognition materials for the ultrasensitive detection of periodontal disease biomarkers *Anal. Bioanal. Chem.* **416** 7305–16
[23] McClements J *et al* 2022 Molecularly imprinted polymer nanoparticles enable rapid, reliable, and robust point-of-care thermal detection of SARS-CoV-2 *ACS Sens.* **7** 1122–31
[24] Garcia Cruz A, Haq I, Cowen T, Di Masi S, Trivedi S, Alanazi K, Piletska E, Mujahid A and Piletsky S A 2020 Design and fabrication of a smart sensor using *in silico* epitope mapping and electro-responsive imprinted polymer nanoparticles for determination of insulin levels in human plasma *Biosens. Bioelectron.* **169** 112536
[25] Cáceres C, Canfarotta F, Chianella I, Pereira E, Moczko E, Esen C, Guerreiro A, Piletska E, Whitcombe M J and Piletsky S A 2016 Does size matter? Study of performance of pseudo-ELISAs based on molecularly imprinted polymer nanoparticles prepared for analytes of different sizes *Analyst* **141** 1405–12
[26] Yucel N, Gulen H and Cakir Hatir P 2022 Molecularly imprinted polymer nanoparticles for the recognition of ellagic acid *J. Appl. Polym. Sci.* **139** e52952
[27] Shen X, Huang C, Shinde S, Jagadeesan K K, Ekström S, Fritz E and Sellergren B 2016 Catalytic formation of disulfide bonds in peptides by molecularly imprinted microgels at oil/water interfaces *ACS Appl. Mater. Interfaces* **8** 30484–91
[28] Heller G T, Mercer-Smith A R and Johal M S 2015 *Protein-Protein Interactions: Methods and Applications* ed C L Meyerkord and H Fu (Springer) pp 153–64
[29] Tsai T-C, Liu C-W, Wu Y-C, Ondevilla N A P, Osawa M and Chang H-C 2019 *In situ* study of EDC/NHS immobilization on gold surface based on attenuated total reflection surface-enhanced infrared absorption spectroscopy (ATR-SEIRAS) *Colloids Surf.* B **175** 300–5
[30] Erol K, Hasabnis G and Altintas Z 2023 A novel nanoMIP-SPR sensor for the point-of-care diagnosis of breast cancer *Micromachines* **14** 1086
[31] Fischer M J E 2010 *Surface Plasmon Resonance: Methods and Protocols* ed N J Mol and M J E Fischer (Humana Press) pp 55–73
[32] Hejazi S M, Erfan M and Mortazavi S A 2013 Precipitation reaction of SDS and potassium salts in flocculation of a micronized megestrol acetate suspension *Iran. J. Pharm. Res.* **12** 239–46
[33] Sengel S B and Sahiner N 2019 Synthesis and characterization of poly(N-(2-mercaptoethyl) acrylamide) microgel for biomedical applications *Polym. Adv. Technol.* **30** 2109–21

[34] Acciaro R, Gilányi T and Varga I 2011 Preparation of monodisperse poly(N-isopropylacrylamide) microgel particles with homogenous cross-link density distribution *Langmuir* **27** 7917–25
[35] Patton J N and Palmer A F 2006 Physical properties of hemoglobin−poly(acrylamide) hydrogel-based oxygen carriers: effect of reaction pH *Langmuir* **22** 2212–21
[36] Neises B and Steglich W 1978 Simple method for the esterification of carboxylic acids *Angew. Chem., Int. Ed. Engl.* **17** 522–4
[37] Tsakos M, Schaffert E S, Clement L L, Villadsen N L and Poulsen T B 2015 Ester coupling reactions—an enduring challenge in the chemical synthesis of bioactive natural products *Nat. Prod. Rep.* **32** 605–32
[38] Sullivan M V, Henderson A, Hand R A and Turner N W 2022 A molecularly imprinted polymer nanoparticle-based surface plasmon resonance sensor platform for antibiotic detection in river water and milk *Anal. Bioanal. Chem.* **414** 3687–96
[39] Cáceres C, Moczko E, Basozabal I, Guerreiro A and Piletsky S 2021 Molecularly imprinted nanoparticles (nanoMIPs) selective for proteins: optimization of a protocol for solid-phase synthesis using automatic chemical reactor *Polymers* **13** 314
[40] Abbas A, Linman M J and Cheng Q 2011 Sensitivity comparison of surface plasmon resonance and plasmon-waveguide resonance biosensors *Sens. Actuators* B **156** 169–75
[41] Chabot V, Miron Y, Grandbois M and Charette P G 2012 Long range surface plasmon resonance for increased sensitivity in living cell biosensing through greater probing depth *Sens. Actuators* B **174** 94–101
[42] Sullivan M V, Clay O, Moazami M P, Watts J K and Turner N W 2021 Hybrid aptamer-molecularly imprinted polymer (aptaMIP) nanoparticles from protein recognition—a trypsin model *Macromol. Biosci.* **21** 2100002
[43] Ashley J, Shukor Y, D'Aurelio R, Trinh L, Rodgers T L, Temblay J, Pleasants M and Tothill I E 2018 Synthesis of molecularly imprinted polymer nanoparticles for α-casein detection using surface plasmon resonance as a milk allergen sensor *ACS Sens.* **3** 418–24
[44] Khan S H, Farkas K, Kumar R and Ling J 2012 A versatile method to measure the binding to basic proteins by surface plasmon resonance *Anal. Biochem.* **421** 385–90
[45] Friguet B, Chaffotte A F, Djavadi-Ohaniance L and Goldberg M E 1985 Measurements of the true affinity constant in solution of antigen-antibody complexes by enzyme-linked immunosorbent assay *J. Immunol. Methods* **77** 305–19
[46] Silva A T, Figueiredo R, Azenha M, Jorge P A S, Pereira C M and Ribeiro J A 2023 Imprinted hydrogel nanoparticles for protein biosensing: a review *ACS Sens.* **8** 2898–920
[47] Mahajan R, Rouhi M, Shinde S, Bedwell T, Incel A, Mavliutova L, Piletsky S, Nicholls I A and Sellergren B 2019 Highly efficient synthesis and assay of protein-imprinted nanogels by using magnetic templates *Angew. Chem., Int. Ed.* **58** 727–30
[48] Stephen A N, Mercer T, Stockburn W, Dennison S R, Readman J E and Reddy S M 2025 Simple size tuning of magnetic nanoparticles using a microwave solvothermal method and their application to facilitate solid-phase synthesis of molecularly imprinted polymers *Mater. Adv.* (https://doi.org/10.1039/D4MA01115E)